ISSN 2072-5981
doi: 10.26907/mrsej

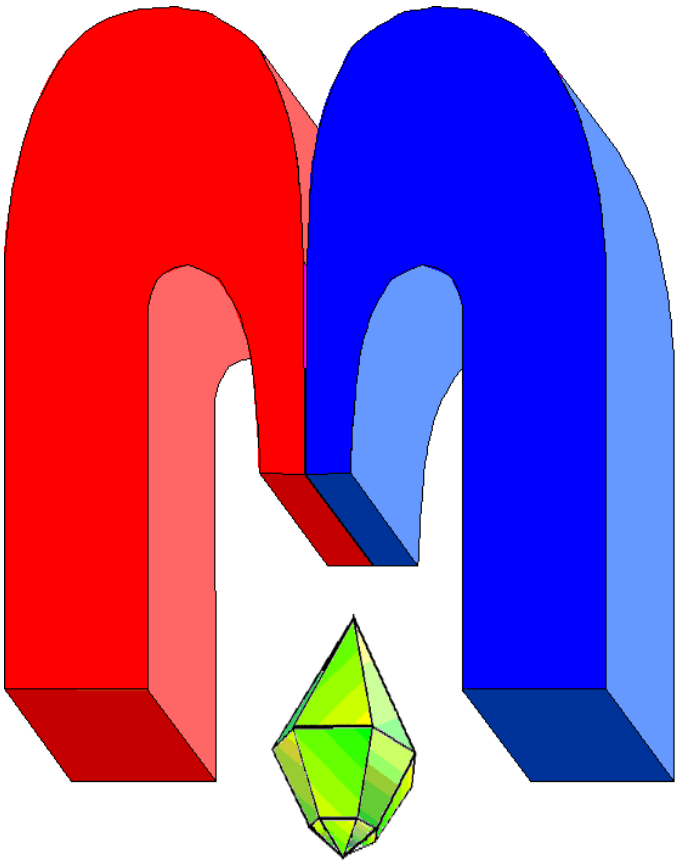

Magnetic Resonance in Solids

Electronic Journal

Volume 27
Issue 3
Article No ***25305***
1-12 pages
2025
doi: **10.26907/mrsej-25305**

http://mrsej.kpfu.ru
http://mrsej.elpub.ru

Established and published by Kazan University*
Endorsed by International Society of Magnetic Resonance (ISMAR)
Registered by Russian Federation Committee on Press (#015140), August 2, 1996
First Issue appeared on July 25, 1997

"***Magnetic Resonance in Solids. Electronic Journal***" (**MRS*ej***) is a peer-reviewed, all electronic journal, publishing articles which meet the highest standards of scientific quality in the field of basic research of a magnetic resonance in solids and related phenomena.

Indexed and abstracted by
Web of Science (ESCI, Clarivate Analytics, from 2015),White List (from 2023) *Scopus* (Elsevier, from 2012), *RusIndexSC* (*eLibrary*, from 2006), *Google Scholar*, *DOAJ*, *ROAD*, *CyberLeninka* (from 2006), *SCImago Journal & Country Rank*, etc.

* Address: "Magnetic Resonance in Solids. Electronic Journal", Kazan Federal University; Kremlevskaya str., 18; Kazan 420008, Russia

† In Kazan University the Electron Paramagnetic Resonance (EPR) was discovered by Zavoisky E.K. in 1944.

Short cite this: *Magn. Reson. Solids* **27**, 25305 (2025) doi: 10.26907/mrsej-25305

Simulation of Rabi oscillations in random clusters of spins deposited on spherical surface

E.I. Kovycheva[1], K.B. Tsiberkin[1,*], V.K. Henner[1,2]

[1]Perm State University, Perm 614068, Russia

[2]University of Louisville, Louisville KY 40292, USA

**E-mail: kbtsiberkin@psu.ru*

(received October 15, 2025; revised November 13, 2025; accepted December 3, 2025; published December 11, 2025)

The study presents results of first-principles modeling of spin dynamics in disordered ensembles of impurity-induced magnetic moments in a carbon spherical structure near 1% concentration of magnetic centers. Averaged signals of Rabi oscillations and their spectra are evaluated using a numerical algorithm based on direct calculation of quantum eigenstates. The Fourier spectrum includes a strong peak around the Rabi frequency and an additional rise in the low-frequency interval. Both peaks demonstrate the standard broadening proportional to the dipole interaction energy. Low-frequency oscillations are observed only for random spin clusters, while regular structures do not produce such dynamics. This effect results from quasi-periodic spin dynamics caused by random distances between particles and, correspondingly, the realization of a set of incommensurate eigenfrequencies in the spin dynamics. Thus, the low-frequency part of the spectrum can be used to characterize spatial disorder in ensembles of spin clusters.

PACS: 67.30.hj, 67.80.Jd, 61.48.+c

Keywords: simulation of spin dynamics, Rabi oscillations, magnetization, spatial disorder.

1. Introduction

In the field of magnetic resonance, doped carbon nanostructures [1, 2] are novel and promising material for analysis. The properties of these materials can be controlled by growing single-domain metal cores within the shells or by depositing magnetic ions on the carbon surface [3–5]. Numerical studies based on density functional theory as well as experiments show that the interaction between the electronic shells of dopant ions and electrons in the carbon lattice induces strong effective magnetic moments due to local change in the π-orbitals of carbon. Their values are close to the Bohr magneton μ_B [6,7]. An indirect exchange also exists in doped carbon, but it decays rapidly due to strong screening and has negligible effect at relevant distances [8, 9]. One of the perspective examples for such studies is the composite of hollow carbon nanoshells 3–5 nm in size [10–12], doped by magnetic ions, e.g., H, N or F. Typical dopant concentration can reach up to 1% or even more, which is much higher than in usual EPR experiments with the concentrations 0.01–0.1% [13, 14]. This determines a characteristic distance between effective magnetic moments induced on sphere about of 2–3 nm, and the dipole energy on the order of 10^{-8} eV. Therefore, modified carbon clusters can be considered as the disordered magnetic with large density of spins. This opens the way to determine disorder parameters from resonance data at high intensity of magnetic interaction, in contrast to the known NMR and NQR studies of disorder in weakly-coupled rarefied systems based on chemical shifts analysis [15, 16]. A few recent studies shows that exploration of system disorder is also effective through the Rabi oscillations of longitudinal magnetization, because they are high-sensitive to variations of the local magnetic fields [17, 18].

Properties of similar spin structures are tough for analysis because of high density of the magnetic moments and significant interactions. The perturbation theory [19] and method of the

moments [20] are inapplicable here. Numerical simulation allows overcoming this difficulties. One of the first known implementations was developed by Henner and Shaposhnikov [21, 22]. First, they evaluate the diagonalizing operator for the Hamiltonian matrix by rotation methods. Then, transition probabilities under a continuous radio-frequency transverse field are obtained from perturbation theory, and a histogram of resonance spectrum is built. Another known approach is based on the approximate evaluation of the time-dependent density matrix [23–25]. A highly detailed realization of this method is developed by Kuprov's group in the SPINACH software [26]. To avoid full matrix evaluation, the software transforms the Hamiltonian and perturbation matrices into block-diagonal structure by excluding the less-probable transitions between system eigenstates. Direct solution of time-dependent Schrödinger equation with non-stationary fields is also applied for the spin decoherence analysis and Rabi problem [13]. This is one of the most flexible methods. However, conservation of the wave-function norm as well as operators unitarity require special numerical approaches with strict control of numerical precision increasing computational costs [27, 28]. Recently, a novel numerical method has been implemented and validated. It builds the time-dependent wavefunction and observables from exact stationary pure states of the spin cluster [29]. An accuracy of their evaluation is limited by only machine precision. Although the method works only with time-independent Hamiltonians, it can be used for simulation of magnetic response under adiabatic perturbations without additional simplifications. Moreover, it allows consideration of harmonic non-stationary field using a rotating reference frame.

Despite the diversity of approaches, evaluation of large-scale quantum problem needs huge operators. For N particles with spin 1/2, the dimension of spin and Hamiltonian matrices is $2^N \times 2^N$. At large N, direct evaluation is impossible even with modern hardware without specific approximations and operator truncation [26]. As an alternative, the averaging method can be applied to systems with the random distribution of magnetic centers. It evaluates resonance signals for a large number of independent small clusters with random spatial distribution of the particles, and builds the mean magnetization and its spectrum. If the number of random realization is large enough, the mean simulated signals match observables in macroscopic ensembles of magnetic clusters [13,21,22]. The averaging method is confirmed by known experimental results for free induction decay as well as Rabi oscillations in diluted compounds, like $CaWO_4$:Yb^{3+}, $CaWO_4$:Er^{3+} and MgO:Mn^{2+} [13, 30].

Previously, the stationary states approach [29] had been used for the analysis of free induction decay of transverse magnetization in ensembles of randomly distributed magnetic moments in a cubic lattice [31]. The FID problem has also been evaluated by this method in regular structures, e.g. linear chains, cubic, and ring clusters of spins [32–34]. In the latter cases, numerical results for single clusters were successfully verified by the theory of moments. Simulated signals of transverse magnetization are in good agreement with the empirical trial functions given in literature [20, 35] and with the experimental data where comparison is possible. On the other hand, averaging over an ensemble of independent clusters with different magnitude of dipole interaction exhibit a direct transition from oscillating signal to monotonic transverse relaxation [31]. Overall, these results confirm the developed method for spin dynamic problems.

In the current study, we present first-principles numerical simulation of Rabi oscillations in clusters of magnetic centers randomly deposited on a diamagnetic sphere in the rotating reference frame with concentration near 1%, using the exact evaluation of stationary eigenstates. Common features of the mean signal and spectra of the dense random spin ensemble are established and analyzed by averaging over a large number of independent random spatial distributions of the

spins.

2. Simulation of Rabi oscillations in disordered spin clusters

Thus, we consider the spherical carbon nanocluster doped with magnetic ions, e.g. H, F or N [10,11]. The dopants are randomly placed on the carbon surface (Figure 1). In the numerical implementation, the azimuthal and polar angles of the dopants are set as random variables with uniform distributions in the intervals $[0, 2\pi]$ and $[0, \pi]$, respectively.

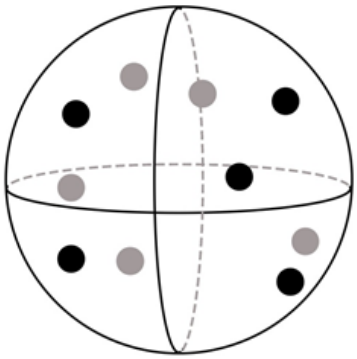

Figure 1. Schematic image of magnetic dopants are randomly distributed on the spherical carbon nanostructure.

We assume that all particles in the cluster have equal spins $S = 1/2$ and identical gyromagnetic ratios γ. In the general case, the dimensionless Hamiltonian of the system is as follows [20]:

$$\frac{\hat{H}}{\hbar\omega_0} = -\mathbf{e}_z \sum_{j=1}^{N} \mathbf{S}_j + p_d \sum_{j<k} \frac{1}{r_{jk}^3} \left(\mathbf{S}_j \cdot \mathbf{S}_k - \frac{3}{r_{jk}^2} (\mathbf{S}_j \cdot \mathbf{r_{jk}})(\mathbf{S}_k \cdot \mathbf{r_{jk}}) \right), \tag{1}$$

where $\omega_0 = \gamma H_0$ is the Larmor frequency in stationary magnetic field $\mathbf{H}_0 = \{0, 0, H_0\}$, $\hbar\omega_0$ is the Zeeman energy of particles, $\mathbf{S}_j$ is the spin operator of j-th particle, $\mathbf{r}_{jk}$ is the radius-vector between particles j and k, $\mathbf{e}_z$ is the unit-vector of z-axis, and p_d is the relative intensity of dipole interaction:

$$p_d = \frac{E_{\text{dip}}}{E_{\text{Zeeman}}} = \frac{\hbar^2\gamma^2}{a_0^3(\hbar\omega_0)}. \tag{2}$$

Here, a_0 is the characteristic distance between particles. It determines the magnitude of dipole interaction. Therefore, we refer the geometrical size of system and coordinates of the particles to this parameter. The vectors $\mathbf{r}_{jk}$ are also scaled to a_0. In addition, all energies are scaled to the Zeeman energy, and time is measured in units of the inverse Larmor frequency, i.e. $[t] = \omega_0^{-1}$.

The external magnetic field includes a constant term $\mathbf{H}_0$, whose direction defines z-axis, and a transverse oscillatory part $\mathbf{H}_1$. Without loss of generality, the transverse field can be described as rotating with frequency Ω:

$$\mathbf{H}_1 = H_1 \{\cos\Omega t, \sin\Omega t, 0\}. \tag{3}$$

In the reference frame rotating with frequency Ω around z-axis, the field (3) becomes constant. Thus, we can use a stationary Hamiltonian in the effective field. There is also a well-established transformation of the longitudinal field component [20]:

$$\mathbf{H} = \left(H_0 - \frac{\Omega}{\gamma} \right) \mathbf{e}_z + H_1 \mathbf{e}_x. \tag{4}$$

If the rotation frequency Ω exactly equals the Larmor frequency ω_0, the longitudinal component vanishes, and the eigenstates structure and their evaluation are simplified.

Additionally, the non-secular part of the dipole interaction in (1) should be omitted in the rotating reference frame. Therefore, we use the truncated Hamiltonian:

$$\frac{\hat{H}}{\hbar\omega_0} = -h_1 \sum_{j=1}^{N} S_j^x + p_d \sum_{j<k} \frac{1 - 3\cos^2\theta_{jk}}{r_{jk}^3} \left(3S_j^z S_k^z - \mathbf{S}_j \cdot \mathbf{S}_k\right), \tag{5}$$

where θ_{jk} is the polar angle between $\mathbf{r}_{jk}$ and field $\mathbf{H}_0$, and $h_1 = H_1/H_0$ is the relative strength of the transverse field.

Full matrix of the Hamiltonian is built from the spin operators represented by tensor products [25]

$$\mathbf{S}_j = I \otimes I \otimes \cdots \otimes \frac{1}{2}\sigma \otimes \cdots \otimes I \otimes I, \tag{6}$$

where I is the identity matrix of 2×2 size and σ is the vector of Pauli matrices placed at the j-th position in the operators product; spin is normalized to $\hbar$. After calculating the eigenvalues E_j and eigenvectors $|\varphi_j\rangle$ of the Hamiltonian, the algorithm expands the initial state $|\Psi(0)\rangle$ over the eigenvectors and evaluates the time-dependent wave function [29]:

$$|\Psi(t)\rangle = \sum_j C_j \exp(-iE_j t)|\varphi_j\rangle, \quad C_j = \langle\Psi(0)|\varphi_j\rangle. \tag{7}$$

In the current problem, the initial state is an adiabatically prepared inverse z-polarization of spin cluster, $M^z(t=0) = -1$.

Finally, the longitudinal magnetization is evaluated using the standard relation:

$$M^z(t) \sim \langle\Psi(t)|S^z|\Psi(t)\rangle. \tag{8}$$

The rotation frequency of transverse field is ω_0, resulting the spin resonance and Rabi oscillations of magnetization with frequency $\omega_R = \gamma H_1$. $M^z(t)$ remains unchanged when returning into the laboratory reference frame.

The algorithm is implemented in Python language using NumPy and LAPACK numerical libraries [36]. It should be noted that there is a strict limitation on the spin ensemble size, because the matrices dimension grows as 2^N. Our hardware permits handling up to $N = 14$ particles, but most simulations were performed with $N = 10 - 12$ as a compromise between system size and computation time.

3. Numerical results

Each random configuration of magnetic centres on the sphere leads to different magnetization dynamics and spectrum structure. Since carbon samples consist of many spheres, the total magnetization can be obtained by averaging the simulated signals [21].

Figure 2 shows the evolution of the longitudinal magnetization of spin ensembles with different N averaged over 100 to 1000 configurations, with varying magnitude of dipole interaction. Figure 3 displays their averaged Fourier spectra.

The total magnetization exhibits a monotonic decay which described well by an exponential law:

$$M^z(t) \sim \cos(\omega_R t) \exp\left(-\frac{t}{T_R}\right), \tag{9}$$

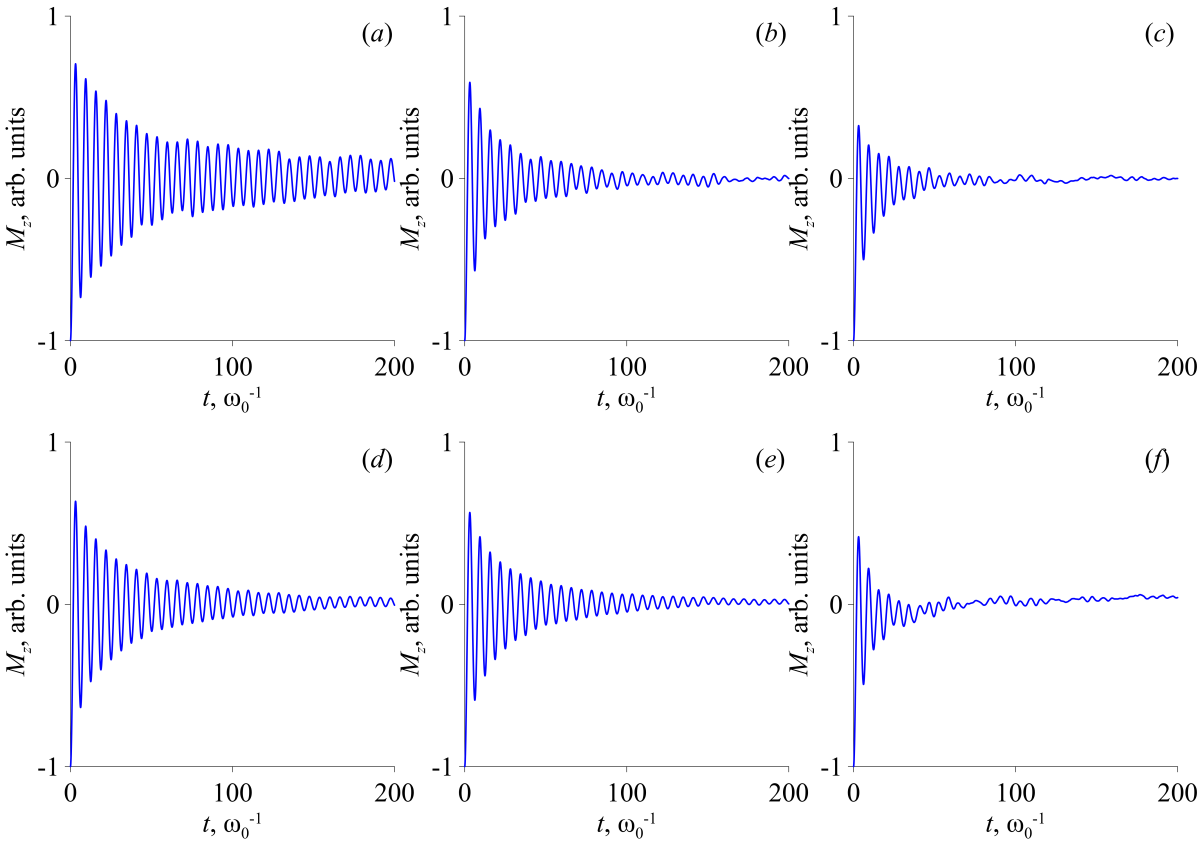

Figure 2. Simulated mean Rabi signals for $N = 10$, 100 random configurations with varying interaction: (a) $p_d = 0.01$, (b) $p_d = 0.025$, (c) $p_d = 0.05$, also for $p_d = 0.05$: (d) $N = 8$, (e) $N = 10$, both include 1000 random spatial structures, and (f) $N = 13$, sum of 150 configurations.

where $T_R \sim (\omega_0 p_d)^{-1}$ is a characteristic damping time, close to the spin-spin relaxation time T_2. The exponential decay appears even with a small number of random realizations of cluster structure. Adding more realization only smooths the signal. Nevertheless, variations in the local dipole field leads to changes in the observed signal and spectrum (Fig. 3). Decay time depends on the dipole interaction magnitude, while the Rabi frequency is determined by transverse field.

In common, this result agrees with simulations of Rabi oscillations as well as experimental data for diluted magnetics reported in literature. For example, we consider $CaWO_4$:Er^{3+} under a 1 mT microwave field (Rabi frequency 55.96 MHz); the static longitudinal field sets the Larmor frequency at 9.7 GHz. These reference values were used by de Raedt [13]. The Er^{3+} ions have a high-anisotropic gyromagnetic ratio, that is 1.25 and 8.38 in *aa*-plane [37]. Referring the characteristic dipole parameter to the lattice constant $a_0 \approx 0.543$ nm, we get $p_d = \omega_{dip}/\omega_0 \approx 0.033$. The dimensionless magnitude of the transverse field is $h_1 \approx 5.77 \cdot 10^{-3}$. Examples of magnetization evaluated in dimensional time (Figures 4,(a), (b)) show good match with known experimental results [13,30]. Figure 4(c) illustrates Rabi oscillations parameters in a fluorinated carbon sphere on a dimensional time scale, for comparison. In that case, the distance between magnetic centers is $0.2-0.3$ nm (concentration is 10^{-2}), and their magnetic moment is μ_B. This yields a high $p_d \approx 0.45$, leading to much faster relaxation and a typical exponential decay signal.

The averaged spectrum of a diluted material contains a single resonance line at the Rabi frequency. As expected, it is broadened proportionally to the dipole-dipole interaction parameter p_d. The height of the main peak also decreases proportionally to p_d due to stronger oscillation

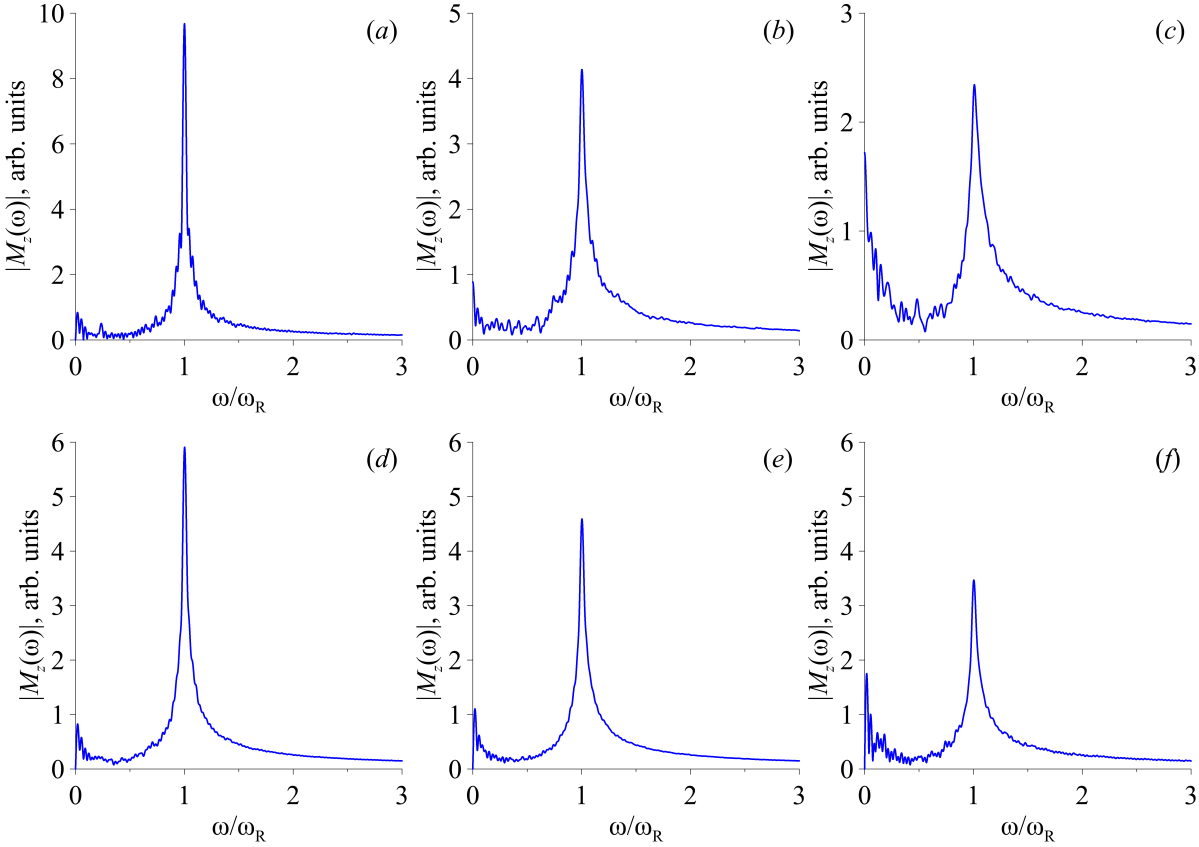

Figure 3. Mean Fourier spectra of Rabi oscillations for $N = 10$, 100 random configurations with varying interaction: (a) $p_d = 0.01$, (b) $p_d = 0.025$, (c) $p_d = 0.05$, also for $p_d = 0.05$: (d) $N = 8$, (e) $N = 10$, both include 1000 random spatial structures, and (f) $N = 13$, sum of 150 configurations.

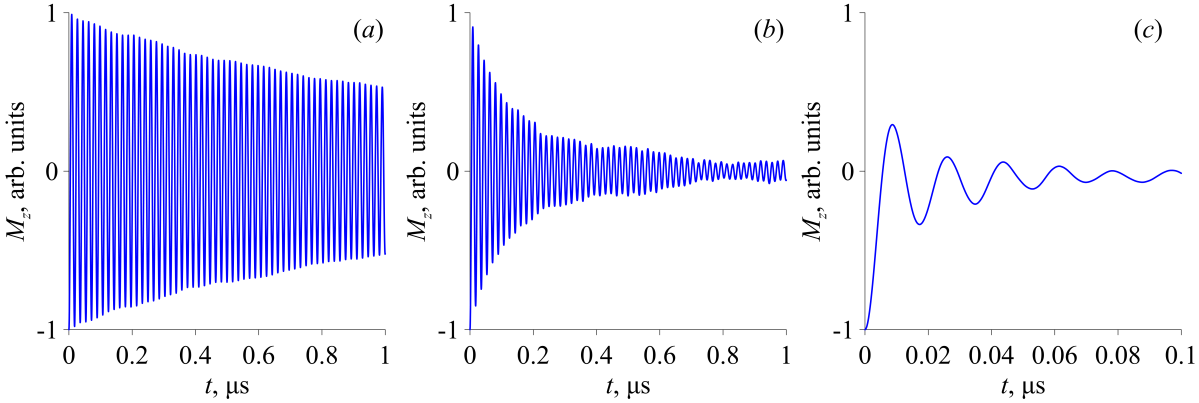

Figure 4. Simulated mean Rabi signals for $N = 8$, 100 random configurations, in dimensional time scale corresponding: $CaWO_4:Er^{3+}$, concentration is (a) 10^{-4}, (b) 10^{-3}, and (c) magnetic moments induces by F atoms deposited at carbon sphere 5 nm in diameter, concentration is 10^{-2}.

damping, which corresponds the signal shape. For small N, dipolar splitting of the main peak can also be observed. However, spectra obtained of dense disordered spin clusters show a significant contribution of low frequency oscillation. For $p_d = 0.05$, the peak height at zero frequency is comparable to that of the main resonance line. This arises from a superposition of slow harmonics present in every random cluster configuration.

This effect is not observed in the spectra of regular spin clusters, particularly elements of

the square lattice (Figure 5). These regular structures exhibits typical signals close to empirical

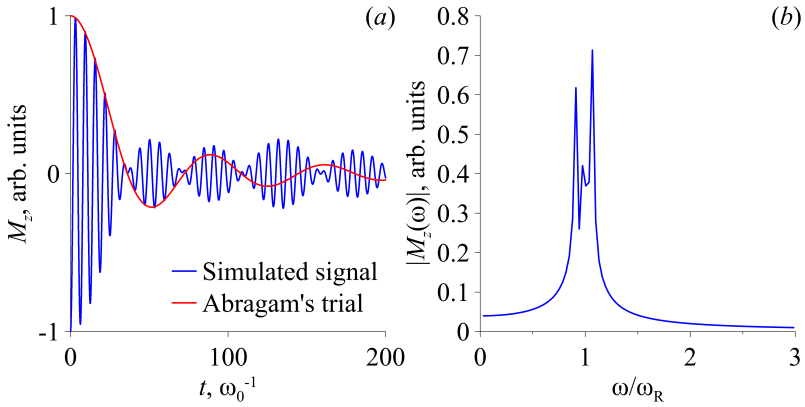

Figure 5. Example of Rabi oscillations with an empirical envelope (a) and its spectrum (b) for 9 particles in square lattice with $p_d = 0.025$.

approximations described in literature. For example, Abragam's trial function [20]

$$M(t) \sim \exp\left(-\frac{a^2t^2}{2}\right)\frac{\sin bt}{bt} \tag{10}$$

corresponds well with the signal of a square lattice element. The given example with $p_d = 0.025$ has $a \approx 0.0042$ and $b \approx 0.087$. The empirical envelope fits the simulated magnetization up to $t \approx 100$. After this point, the signal appears a beating between two close frequencies. This is supported by two strong peaks in signal spectrum around the Rabi frequency (see Figure 5b).

4. Analytical estimates and discussion

Before discussing possible reasons for the low-frequency rise in the spectrum, we consider the solution for Rabi oscillations in a system of two spins. There is a significant difference between the structures of Hamiltonian matrices for free induction decay and Rabi magnetization reversals.

For free induction decay in the laboratory reference frame, the Zeeman energy operator is represented by the pure diagonal matrix S^z. For two spins it is as follows:

$$S^z = \begin{pmatrix} -1 & 0 & 0 & 0 \\ 0 & 0 & 0 & 0 \\ 0 & 0 & 0 & 0 \\ 0 & 0 & 0 & 1 \end{pmatrix}, \ |\varphi_1\rangle = \begin{pmatrix} 1 \\ 0 \\ 0 \\ 0 \end{pmatrix}, \ |\varphi_2\rangle = \begin{pmatrix} 0 \\ 1 \\ 0 \\ 0 \end{pmatrix}, \ |\varphi_3\rangle = \begin{pmatrix} 0 \\ 0 \\ 1 \\ 0 \end{pmatrix}, \ |\varphi_4\rangle = \begin{pmatrix} 0 \\ 0 \\ 0 \\ 1 \end{pmatrix}. \tag{11}$$

It has a simple structure of eigenvectors. States φ_2 and φ_3 are degenerate with common energy $E_{2,3} = 0$. Adding of the dipole interaction lifts the degeneracy, causing state mixing:

$$|\tilde{\varphi}_2\rangle = \frac{1}{\sqrt{2}}(|\varphi_2\rangle + |\varphi_3\rangle), \quad |\tilde{\varphi}_3\rangle = \frac{1}{\sqrt{2}}(|\varphi_2\rangle - |\varphi_3\rangle). \tag{12}$$

In constast, for Rabi oscillations the Zeeman term is defined by the matrix S^x:

$$S^x = \begin{pmatrix} 0 & 1/2 & 1/2 & 0 \\ 1/2 & 0 & 0 & 1/2 \\ 1/2 & 0 & 0 & 1/2 \\ 0 & 1/2 & 1/2 & 0 \end{pmatrix},$$
$$|\varphi_1\rangle = \frac{1}{\sqrt{2}} \begin{pmatrix} 1 \\ 0 \\ 0 \\ -1 \end{pmatrix}, \; |\varphi_2\rangle = \frac{1}{\sqrt{2}} \begin{pmatrix} 0 \\ 1 \\ -1 \\ 0 \end{pmatrix}, \; |\varphi_3\rangle = \frac{1}{2} \begin{pmatrix} 1 \\ 1 \\ 1 \\ 1 \end{pmatrix}, \; |\varphi_4\rangle = \frac{1}{2} \begin{pmatrix} 1 \\ -1 \\ -1 \\ 1 \end{pmatrix}. \tag{13}$$

The off-diagonal terms of S^x produce a more complex structure of eigenstates and mix different frequencies within the total magnetization (9).

Moreover, there is a competition with the dipole part of Hamiltonian (5), where diagonal operator $S^z \dot{S}^z$ dominates:

$$\hat{H}_{dip} = \frac{1}{4} f p_d \begin{pmatrix} 1 & 0 & 0 & 0 \\ 0 & -1 & -1 & 0 \\ 0 & -1 & -1 & 0 \\ 0 & 0 & 0 & 1 \end{pmatrix}, \tag{14}$$

where $f = 1 - 3\cos^2\theta_{12}$. In the general case, analytical formulas for eigenvalues and eigenvectors of the full Hamiltonian are large even for two particles. Nevertheless, it can be simplified because of small p_d:

$$E_1 \approx -1 - \frac{f p_d}{8}, \quad E_2 = 0, \quad E_3 = \frac{f p_d}{4}, \quad E_4 \approx 1 - \frac{f p_d}{8}, \tag{15}$$

the energy values are expanded up to linear order in the dipole parameter. The corresponding eigenstates are as follows:

$$|\varphi_1\rangle \approx \frac{1}{1+\lambda_+} \begin{pmatrix} 1 \\ \lambda_+ \\ \lambda_+ \\ 1 \end{pmatrix}, \; |\varphi_2\rangle = \frac{1}{\sqrt{2}} \begin{pmatrix} 0 \\ 1 \\ -1 \\ 0 \end{pmatrix}, \; |\varphi_3\rangle = \frac{1}{\sqrt{2}} \begin{pmatrix} 1 \\ 0 \\ 0 \\ 1 \end{pmatrix}, \; |\varphi_4\rangle \approx \frac{1}{1+\lambda_-} \begin{pmatrix} 1 \\ -\lambda_- \\ -\lambda_- \\ 1 \end{pmatrix},$$
$$\lambda_\pm = 1 \pm \frac{3 f p_d}{8}. \tag{16}$$

The initial state of inverted M^z is given by vector $|\Psi(t=0)\rangle = (0,0,0,1)^T$, therefore the expansion coefficients C_j (see (7)) are as follows:

$$C_1 = \frac{1}{1+\lambda_+}, \quad C_2 = 0, \quad C_3 = -\frac{1}{\sqrt{2}}, \quad C_4 = \frac{1}{1+\lambda_-}. \tag{17}$$

Thus, three of the eigenstates (16) contribute equally to the full wave function (7) and the observed magnetization (8). Finally, $M^z(t)$ for $N = 2$ in the small p_d limit becomes

$$M^z_{N=2}(t) \approx \lambda_+ \cos\lambda_- t + \lambda_- \cos\lambda_+ t. \tag{18}$$

For example, if the spin pair is along z-axis ($\theta_{12} = 0$) with $p_d = 0.05$, the energy levels, wave

function and magnetization are as follows:

$$E_1 \approx -0.978, \quad E_2 = 0.00, \quad E_3 = 0.05, \quad E_4 = 1.03,$$
$$|\Psi(t)\rangle \approx \begin{pmatrix} 0.23\exp(-iE_4t) - 0.5\exp(-iE_3t) + 0.27\exp(-iE_1t) \\ -0.25\exp(-iE_4t) + 0.25\exp(-iE_1t) \\ -0.25\exp(-iE_4t) + 0.25\exp(-iE_1t) \\ 0.23\exp(-iE_4t) + 0.5\exp(-iE_3t) + 0.27\exp(-iE_1t) \end{pmatrix}, \tag{19}$$
$$M^z_{N=2}(t) \approx 1.08\cos(0.93t) + 0.92\cos(1.08t).$$

The elements of the wave function consist of a few eigenstates. For free induction decay, the eigenstates are not mixed, and each element of $|\Psi(t)\rangle$ includes only one $\exp(-iE_jt)$.

Thereby, the leading terms of the longitudinal magnetic moment of two spins in the rotating reference frame include only two harmonics around the Rabi frequency with a dipole shift. No low-frequency terms appear. Nevertheless, we assume that low-frequency dynamics is determined by the off-diagonal terms of S^x and $\hat{H}_{dip}$ operators in higher dimensions. Direct evaluation of the wave function and magnetization shows that the energy spectra of random clusters include several closely spaced levels. Transitions between these levels produce terms $\cos(\omega_R p_d t)$ in the magnetization signal. Since a random cluster can be considered as a set of spin pairs with varying interaction, every specific spectrum has a few peaks near zero corresponding to these pairs. A few examples are shown in Figure 6. Averaging the signal spectrum over a large number of

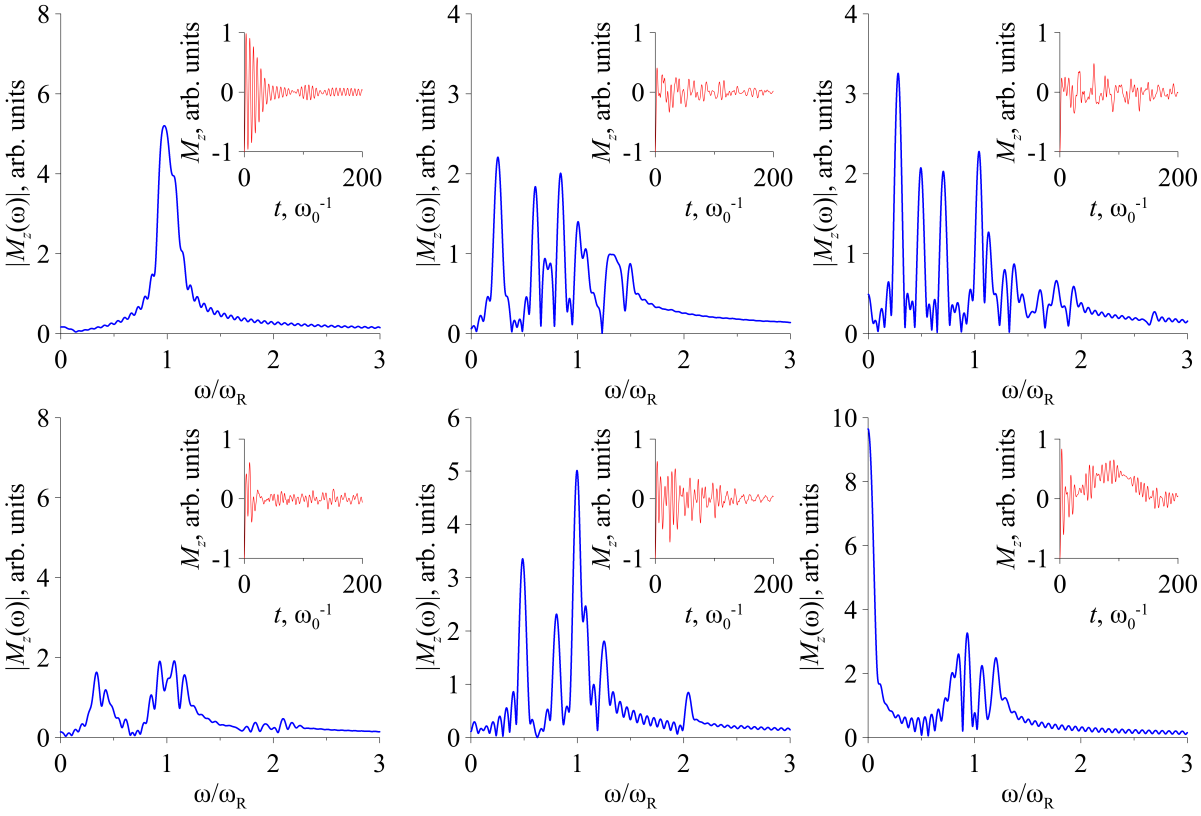

Figure 6. Examples of the Fourier spectra of Rabi oscillations for $p_d = 0.05$ and 10 particles for random realizations; insets exhibit the magnetization evolution corresponding each spectrum.

spatial configurations smooths the spectrum and produces a visible rise near zero frequency in the total spectrum (see Figure 3). These additional peaks occur due to strong irregularities of the eigenfrequencies in random dense clusters, while in regular cluster all of them are localized

near ω_R. Spectral variations are well-illustrated by the "zoo" of possible signal waveforms (see Figure 6), which have a rather different time scales. Increasing the number of realizations (see Figure 2) enhances the smoothing of the mean signal and spectrum, making statistical analysis of disorder possible.

In addition, when the spin cluster includes randomly spaced particles, the interaction terms also have random magnitudes. In the general case, this produces a set of incommensurable frequencies. Therefore, quasi-periodic motion arises here, in accordance with the general principles of nonlinear systems theory [38]. The continuous Fourier spectrum of such regimes shows that they can be considered as a form of noise. The spectrum of spin quasi-periodic motion exhibits the same rise near zero as we observe in our simulations [39]. On the other hand, regular spin clusters do not enter such dynamic regime, because the main eigenfrequencies in regular lattice are rationally related. In that case, the system's motion always remains periodic.

5. Conclusion

We performed a series of first-principles numerical simulations of spin ensembles randomly distributed on spherical nanostructures under the oscillating transverse field. In the rotating reference frame, Rabi oscillations of longitudinal magnetization are observed. Every unique random spatial configuration of the spin cluster produces irregular signals and spectra. However, the magnetization averaged over many configurations shows a smooth decay close to exponential, characterized by the time $T_R \approx T_2$.

The averaged Fourier spectrum, besides the broadened peak at the Rabi frequency, shows a rise near zero frequencies. This effect is not observed for spin clusters with regular structures. Excitation of low-frequency spin dynamics results from cluster disorder. Dipole interactions between randomly deposited particles produce multiple incommensurable eigenfrequencies, so the spin cluster enters a quasi-periodic regime with many low-frequency harmonics. Thus, the current study has a fundamental interest in the field of chaotic dynamics of quantum spins.

Additionally, first-principal modeling provides a basis for disorder analysis in spin systems. The shape and fine structure of the main peak and zero-frequency rise in the spectrum contain information about the spatial distribution of particles. Since low-frequency oscillations are observed only in random structures, this part of the spectrum can be useful for disorder analysis. Accumulating simulated data will allow evaluation of the particle distribution parameters from signals. Further, it can be applied to real physical experiments.

References

1. Rao C. N. R., Seshadri R., Govindaraj A., Sen R. *Material Science and Engineering* **15**, 209 (1995)
2. Burchell T. D. *Carbon Materials for Advanced Technologies*, Amsterdam, Elsevier (1999)
3. An K. H., Heo J. G., Jeon K. G., Bae D. J., Jo C., Yang C. W., Park C.-Y., Lee Y. H., Chung Y. S. *Applied Physics Letters* **80**, 4235 (2002)
4. Nourbakhsh A., Cantoro M., Vosch T., Pourtois G., Clemente F., van der Veen M. H., Hofkens J., Heyns M. M., De Gendt S., Sels B. F. *Nanotechnology* **21**, 435203 (2010)
5. Gargiulo F., Autes G., Virk N., Barthel S., Rösner M., Toller L. R. M., Wehling T. O., Yazyev O. V. *Physical Review Letters* **113**, 246601 (2014)
6. Yazyev O. V., Helm L. *Physical Review B* **75**, 125408 (2007)

7. Berashevich J., Chakraborty T. *Nanotechnology* **21**, 355201 (2010)
8. Saremi S. *Physical Review B* **76**, 184430 (2007)
9. Rudenko A. N., Keil F. J., Katsnelson M. I., Lichtenstein A. I. *Physical Review B* **88**, 081405(R) (2013)
10. Rudakov G. A., Sosunov A. V., Ponomarev R. S., Henner V. K., Shamim Reza Md., Sumanasekera G. *Physics of the Solid State* **60**, 167 (2018)
11. Rudakov G. A., Tsiberkin K. B., Ponomarev R. S., Henner V. K., Ziolkowska D. A., Jasinski J. B., Sumanasekera G. *Journal of Magnetism and Magnetic Materials* **427**, 34 (2019)
12. Germov A. Yu., Prokopyev D. A., Mikhalev K. N., Goloborodskiy B. Yu., Uimin M. A., Yermakov A. E., Konev A. S., Minin A. S., Novikov S. T., Gaviko V. S., Murzakaev A. M. *Materials Today Communications* **27**, 102382 (2021)
13. de Raedt H., Barbara B., Miyashita S., Michielsen K., Bertaina S., Gambarelli S. *Physical Review B* **85**, 014408 (2012)
14. Baibekov E., Kurkin I., Gafurov M., Endeward B., Rakhmatullin R., Mamin G. *Journal of Magnetic Resonance* **209**, 61 (2011)
15. Moran R. F., Dawson D. M., Ashbrook S. E. *International Review in Physical Chemistry* **36**, 39 (2017)
16. Chen K. *International Journal of Molecular Sciences* **21**, 5666 (2020)
17. Khomitsky D. V., Gulyaev L. V., Sherman E. Ya. *Physical Review B* **85**, 125312 (2012)
18. Glenn R., Baker W. J., Boehme C., Raikh M. E. *Physical Review B* **87**, 155208 (2013)
19. Dzheparov F. S., Kaganov V. I., Khenner E. K. *Journal of Experimental and Theoretical Physics* **85**, 325 (1997)
20. Slichter C. P. *Principles of Magnetic Resonance*, Springer, Berlin (1990)
21. Henner E. K., Shaposhnikov I. G. *Radiospectroscopy* **10**, 74 (1976) [In Russian]
22. Henner E., Shaposhnikov I., Bonis B., Sardos R. *Journal of Magnetic Resonance* **32**, 107 (1978)
23. Bengs C., Levitt M. H. *Magnetic Resonance in Chemistry* **56**, 374 (2018)
24. Jeschke G. *Journal of Magnetic Resonance Open* **14**, 100094 (2023)
25. Kuprov I. *Spin*, Springer, Cham (2023)
26. Kuprov I. *Journal of Magnetic Resonance* **209**, 31 (2011)
27. Gharibnejad H., Schneider B. I., Leadingham M., Schmale H. J. *Computer Physics Communications* **252**, 106808 (2020)
28. van Dijk W. *Americal Journal of Physics* **91**, 826 (2023)
29. Henner V., Klots A., Nepomnyashchy A., Belozerova T. *Applied Magnetic Resonance* **52**, 859 (2021)
30. Baibekov E. I., Gafurov M. R., Zverev D. G., Kurkin I. N., Rodionov A. A., Malkin B. Z., Barbara B. *Physical Review B* **95**, 064427 (2017)
31. Tsiberkin K. B. *The European Physical Journal B* **96**, 70 (2023)
32. Kovycheva E. I., Tsiberkin K. B. *Bulletin of Perm University. Physics* **2**, 26 (2022) [In Russian]

33. Tsiberkin K. B., Kovycheva E. I. *Applied Magnetic Resonance* **55**, 565 (2024)

34. Tsiberkin K. B., Kovycheva E. I., Henner V. K. *Bulletin of the Russian Academy of Sciences: Physics* **89**, 1707 (2025)

35. Jensen S. J. K., Platz O. *Physical Review B* **77**, 31 (1973)

36. Millman K. J., Aivazis M. *Computing in Science and Engineering* **13**, 9 (2011)

37. Ourari S., Dusanowski L., Horvath S. P., Uysal M. T., Phenicie C. M., Stevenson P., Raha M., Chen S., Cava R. J., de Leon N. P., Thompson J. D. *Nature* **620**, 977 (2023)

38. Kuznetsov A. P., Migunova N. A., Sataev I. R., Sedova Y. V., Turukina L. V. *Regular and Chaotic Dynamics* **20**, 189 (2015)

39. Velez J. A., Perez L. M., Pizarro A. E., Pedraja-Rejas L., Suarez O. J., Hernandez-Garcia R., Barrientos R. J., Bragard J., Laroze D., Otxoa R. M. *Communications in Nonlinear Science and Numerical Simulation* **149**, 108942 (2025)